Nonlinear Dyn (2007) 49:349–359
DOI 10.1007/s11071-006-9127-8

ORIGINAL ARTICLE

Stability analysis for milling process

X.-H. Long · B. Balachandran

Received: 11 January 2002 / Accepted: 27 August 2004 / Published online: 5 January 2007

Abstract In this article, the stability of a milling process is studied by using a semi-discretization method. The model of the workpiece–tool system includes loss-of-contact effects between the workpiece and the tool and time-delay effects associated with the chip-thickness variation. In addition, feed-rate effects are also considered. The governing system of equations is a non-autonomous, delay-differential system with time-periodic coefficients. Stability of periodic orbits of this system is studied to predict the onset of chatter and numerical evidence is provided for period-doubling bifurcations and secondary Hopf bifurcations. Stability charts generated using the semi-discretization method are found to compare well with the corresponding results obtained through time-domain simulations.

Keywords Stability · Milling process · Time delay · Chatter

1 Introduction

During a milling process, chatter is an undesired relative vibration between the workpiece and the tool that can result in poor accuracy and tool wear. This undesired state of vibration can also limit the material remove rate, which, in turn, results in a low production rate. Hence, considerable attention has been devoted to understand the chatter mechanisms, predict the onset of chatter, and suppress the chatter. As in self-excited systems (e.g. [1]), there is a regenerative effect in a milling process. This effect is in the form of a time-delay effect in the governing equations, and the physical basis for this effect is the cutting forces in the workpiece–tool system. This force depends on the chip thickness, which is determined not only by the present state of motion of the workpiece–tool system but also by the past state of motion of this system. In the context of milling processes, considerable research on chatter due to this time-delay effect has been carried out [2–9].

As discussed in the studies of Balachandran [9], Balachandran and Zhao [10], Zhao and Balachandran [11], and Balachandran and Gilsinn [12], in general, the governing system of equations of a milling process is a nonlinear, non-homogeneous, delay-differential system with time-periodic coefficients. Over the years, this system of equations have been approximated on a physical basis as well as a mathematical basis to determine the stability of motions of the workpiece–tool system. These approximations are to do with consideration of nonlinearities, time-periodic nature of the cutting-force coefficients, and the feed terms. For example, if one does not consider multiple regenerative effects, loss-of-contact dynamics, friction, structural nonlinearities, and other sources of nonlinearities, then, the resulting

X.-H. Long
The State Key Lab of Vibration, Shock & Noise Shanghai Jiao Tong University, Shanghai 200240, P R China

B. Balachandran (✉)
Department of Mechanical Engineering, University of Maryland, College Park, MD 20742, U.S.A.

system of equations is linear [2, 4, 5, 7, 8]. Tlusty and Polacek [2] presented a frequency-domain approach based on transfer functions between the system displacements and the cutting forces to determine the instability due to the regenerative effect. In milling processes, the orientations of the cutting forces and chip thickness are the explicit periodic functions of time. If the cutting forces are averaged over the period of contact time of each cutter with the workpiece, then the resulting system of delay-differential equations no longer has time-periodic coefficients but rather constant coefficients. This type of averaging was carried out in the Opitz et al. [4] who examined the stability of a face milling process and also in the work of Altintas and Budak [8]. Prior to the stability analysis, Sridhar et al. [5] dropped the feed terms from their model and then studied the stability of the zero solution of the resulting linear, homogeneous delay-differential system with periodic coefficients. Hahn [13] presented an extension of Floquet's theorem for delay-differential equations with periodic coefficients. This provided a basis for the work of Sridhar et al., who numerically computed the fundamental matrix and the eigenvalues of this matrix. In the study of Minis and Yanushevsky [7], as in previous studies [5, 8], milling operations with straight fluted cutters are considered. They used Floquet theory to determine the stability of the zero solution of a linear, homogeneous delay-differential system. The periodic terms were expanded by using a Fourier expansion with the basic frequency defined by the spindle speed. The Hill's determinant [1] was obtained and the zeroth-order and first-order truncations of the resulting characteristic equation were used in determining the stability charts in the space of spindle speed and depth of cut.

In the work of Hanna and Tobias [6], face milling processes were considered and modeled by using structural nonlinearities and cutting-force nonlinearities. Quadratic and cubic nonlinearities were included in a delay-differential system with constant coefficients, and the stability of the zero solution of this system was studied. Unlike the model used by Hanna and Tobias [6], the models used by Sridhar et al. [5], Minis and Yanushevsky [7], and Altintas and Budak [8] are linear. While these linear models are useful for predicting the onset of chatter, they are not suited for understanding the nature of the instability as well as post-instability motions. In the work of Balachandran and Zhao [10] and Zhao and Balachandran [11], loss-of-contact nonlinearities and feed rate effects are considered. They pointed out that linear models can provide quite accurate stability predictions for high-immersion milling operations but inaccurate stability predictions for low-immersion operations. Stability of these operations in the space of spindle speed and depth of cut can be constructed through time-domain simulations of this nonlinear system. However, for determining the type of instability of the periodic motion of this nonlinear, non-homogeneous, non-autonomous, delay-differential system, numerical schemes with an analytical basis are required. To this end, the semi-discretization scheme is used here. This scheme has been shown to be an efficient numerical scheme for studying the stability of the zero solution of non-autonomous systems with a continuous time delay [14, 15].

The primary contribution of this article is in the formulation and use of semi-discretization method for study of stability of periodic motions of workpiece–tool systems associated with milling operations. In formulating this method, an extension has been made to handle cases with multiple time delays. Numerical evidence for bifurcations is also shown by examining the Poincaré sections of periodic motions. The model used in this article is discussed in Section 2, and stability analysis is detailed in Section 3. Results and discussion are presented in Section 4.

2 Governing equations of workpiece–tool system

In this section, the model developed by Balachandran and Zhao [10] is revisited, features of this model are discussed, and a state-space form of the governing equations suitable for stability analysis is formulated. In Fig. 1, a multi-degree-of-freedom system representative of a workpiece–tool system is illustrated for milling operations with a cylindrical end mill. The cutting tool has a radius R, N flutes, and a helix angle η. For convenience, the X-direction is oriented along the feed direction of cutter, and the feed rate is specified by f. The governing equations of motion are of the form [10, 11]

$$\begin{aligned} m_x\ddot{q}_x(t) + c_x\dot{q}_x(t) + k_x q_x(t) &= F_x(t;\tau_1,\tau_2)\\ m_y\ddot{q}_y(t) + c_y\dot{q}_y(t) + k_y q_y(t) &= F_y(t;\tau_1,\tau_2)\\ m_u\ddot{q}_u(t) + c_u\dot{q}_u(t) + k_u q_u(t) &= F_u(t;\tau_1,\tau_2)\\ m_v\ddot{q}_v(t) + c_v\dot{q}_v(t) + k_v q_v(t) &= F_v(t;\tau_1,\tau_2) \end{aligned} \tag{1}$$

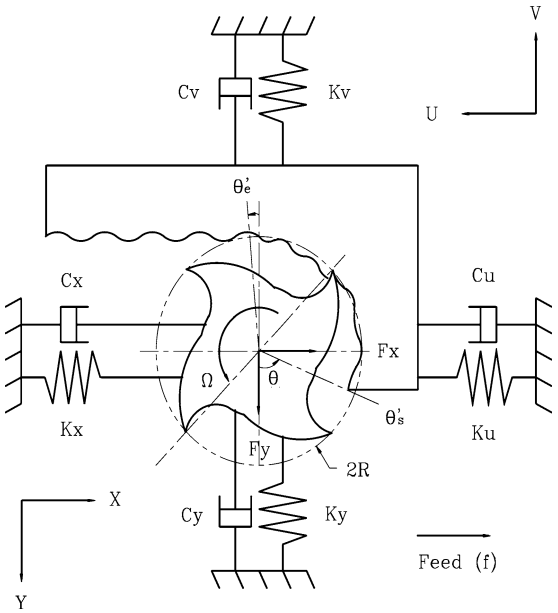

Fig. 1 Workpiece–tool system model

where the tool has 2 degrees of freedom, and the workpiece has 2 degrees of freedom. The cutting force components, which appear on the right-hand side of the equations, are time periodic functions. Furthermore, the discrete time delays τ_1 and τ_2 are introduced in the governing equations through the cutting force components. As discussed later in this section, these delays depend on the feed rate and the spindle rotation speed. The dependence of the cutting forces on the system states are not explicitly shown in Equation (1).

In the cutting zone $\theta'_s < \theta(i,t,z) < \theta'_e$, when the ith cutting tooth is in contact with workpiece, the corresponding cutting force components are given by

$$\begin{Bmatrix} F_x^i(t;\tau_1,\tau_2) \\ F_y^i(t;\tau_1,\tau_2) \end{Bmatrix} = \begin{bmatrix} \kappa_{11}^i(t) & \kappa_{12}^i(t) \\ \kappa_{21}^i(t) & \kappa_{22}^i(t) \end{bmatrix} \begin{Bmatrix} A(t;\tau_1) \\ B(t;\tau_2) \end{Bmatrix} + \begin{bmatrix} c_{11}^i(t) & c_{12}^i(t) \\ c_{21}^i(t) & c_{22}^i(t) \end{bmatrix} \begin{Bmatrix} \dot{A}(t;\tau_1) \\ \dot{B}(t;\tau_2) \end{Bmatrix} \quad (2)$$

where the relative displacement functions are given by

$$\begin{aligned} A(t;\tau_1) &= q_x(t) - q_x(t-\tau_1) \\ &\quad + q_u(t) - q_u(t-\tau_1) + f\tau_1 \\ B(t;\tau_2) &= q_y(t) - q_y(t-\tau_2) + q_v(t) - q_v(t-\tau_2) \end{aligned} \quad (3)$$

When a cutting flute is outside the cutting zone, then the cutting force components associated with this flute are zero. In addition, when the dynamic uncut chip thickness associated with the ith flute is zero, then there is no contact between the workpiece and the corresponding cutter flute. The corresponding cutting force components are zero when there is loss of contact, i.e.,

$$\begin{Bmatrix} F_x^i(t;\tau_1,\tau_2) \\ F_y^i(t;\tau_1,\tau_2) \end{Bmatrix} = \mathbf{0} \quad (4)$$

Carrying out a summation over the N cutting flutes, the cutting force components are determined to be

$$\begin{aligned} \begin{Bmatrix} F_x(t;\tau_1,\tau_2) \\ F_y(t;\tau_1,\tau_2) \end{Bmatrix} &= \sum_{i=1}^{N} \begin{Bmatrix} F_x^i(t;\tau_1,\tau_2) \\ F_y^i(t;\tau_1,\tau_2) \end{Bmatrix} \\ &= \begin{bmatrix} \kappa_{11}(t) & \kappa_{12}(t) \\ \kappa_{21}(t) & \kappa_{22}(t) \end{bmatrix} \begin{Bmatrix} A(t;\tau_1) \\ B(t;\tau_2) \end{Bmatrix} \\ &\quad + \begin{bmatrix} c_{11}(t)\ c_{12}(t) \\ c_{21}(t)\ c_{22}(t) \end{bmatrix} \begin{Bmatrix} \dot{A}(t;\tau_1) \\ \dot{B}(t;\tau_2) \end{Bmatrix} \end{aligned} \quad (5)$$

In addition, from Newton's third law of motion, the forces acting on the workpiece can be determined as

$$\begin{Bmatrix} F_u(t;\tau_1,\tau_2) \\ F_v(t;\tau_1,\tau_2) \end{Bmatrix} = \begin{Bmatrix} F_x(t;\tau_1,\tau_2) \\ F_y(t;\tau_1,\tau_2) \end{Bmatrix} \quad (6)$$

In the previous studies [3–9], the feed rate is assumed to be very small compared to the cutting velocity and the tool-pass period along the X- and Y-directions is taken to be equal to the cutting tooth period T. When, the feed rate is significant, the tool pass period is likely to depend on the feed rate. To capture this dependence, as an approximation, the time delay along the X-direction is assumed to be different from the time delay along the Y-direction, and these delays are determined as follows. Let the tool-pass period along the X-direction be

$$\tau_1 = T = \frac{1}{N\Omega} \quad (7)$$

where Ω is the spindle speed. Then, based on quasi-static approximations, the tool-pass period along the Y-direction can be determined as

$$\tau_2 = \frac{4\pi R}{N(4\pi\Omega R + f)} \quad (8)$$

On substituting Equations (4)–(6) into Equations (1), the resulting system is

$$\begin{aligned}\mathbf{M}\ddot{\mathbf{q}}(t) + [\mathbf{C} - \hat{\mathbf{C}}(t)]\dot{\mathbf{q}}(t) + [\mathbf{K} - \hat{\boldsymbol{\kappa}}(t)]\mathbf{q}(t) \\ = -\hat{\mathbf{C}}_1(t)\dot{\mathbf{q}}(t-\tau_1) \\ -\hat{\mathbf{C}}_2(t)\dot{\mathbf{q}}(t-\tau_2) - \hat{\boldsymbol{\kappa}}_1(t)\mathbf{q}(t-\tau_1) \\ -\hat{\boldsymbol{\kappa}}_2(t)\mathbf{q}(t-\tau_2) + \bar{\boldsymbol{\kappa}} f\tau_1 \end{aligned} \tag{9}$$

where the different matrices are given by

$$\mathbf{M} = \begin{bmatrix} m_x & 0 & 0 & 0 \\ 0 & m_y & 0 & 0 \\ 0 & 0 & m_u & 0 \\ 0 & 0 & 0 & m_v \end{bmatrix} \tag{10}$$

$$\mathbf{C} = \begin{bmatrix} c_x & 0 & 0 & 0 \\ 0 & c_y & 0 & 0 \\ 0 & 0 & c_u & 0 \\ 0 & 0 & 0 & c_v \end{bmatrix} \tag{11}$$

$$\mathbf{K} = \begin{bmatrix} k_x & 0 & 0 & 0 \\ 0 & k_y & 0 & 0 \\ 0 & 0 & k_u & 0 \\ 0 & 0 & 0 & k_v \end{bmatrix} \tag{12}$$

$$\hat{\mathbf{C}}(t) = \hat{\mathbf{C}}_1(t) + \hat{\mathbf{C}}_2(t) \tag{13}$$

$$\hat{\mathbf{C}}_1(t) = \begin{bmatrix} c_{11}(t) & 0 & c_{11}(t) & 0 \\ c_{21}(t) & 0 & c_{21}(t) & 0 \\ c_{11}(t) & 0 & c_{11}(t) & 0 \\ c_{21}(t) & 0 & c_{21}(t) & 0 \end{bmatrix} \tag{14}$$

$$\hat{\mathbf{C}}_2(t) = \begin{bmatrix} 0 & c_{12}(t) & 0 & c_{12}(t) \\ 0 & c_{22}(t) & 0 & c_{22}(t) \\ 0 & c_{12}(t) & 0 & c_{12}(t) \\ 0 & c_{22}(t) & 0 & c_{22}(t) \end{bmatrix} \tag{15}$$

$$\hat{\boldsymbol{\kappa}}(t) = \hat{\boldsymbol{\kappa}}_1(t) + \hat{\boldsymbol{\kappa}}_2(t) \tag{16}$$

$$\hat{\boldsymbol{\kappa}}_1(t) = \begin{bmatrix} \kappa_{11}(t) & 0 & \kappa_{11}(t) & 0 \\ \kappa_{21}(t) & 0 & \kappa_{21}(t) & 0 \\ \kappa_{11}(t) & 0 & \kappa_{11}(t) & 0 \\ \kappa_{21}(t) & 0 & \kappa_{21}(t) & 0 \end{bmatrix} \tag{17}$$

$$\hat{\boldsymbol{\kappa}}_2(t) = \begin{bmatrix} 0 & \kappa_{12}(t) & 0 & \kappa_{12}(t) \\ 0 & \kappa_{22}(t) & 0 & \kappa_{22}(t) \\ 0 & \kappa_{12}(t) & 0 & \kappa_{12}(t) \\ 0 & \kappa_{22}(t) & 0 & \kappa_{22}(t) \end{bmatrix} \tag{18}$$

$$\bar{\boldsymbol{\kappa}}(t) = \begin{Bmatrix} \kappa_{11}(t) \\ \kappa_{21}(t) \\ \kappa_{11}(t) \\ \kappa_{21}(t) \end{Bmatrix} \tag{19}$$

Introducing the state vector,

$$\mathbf{Q} = \begin{Bmatrix} \mathbf{q} \\ \dot{\mathbf{q}} \end{Bmatrix} \tag{20}$$

Equation (9) can be rewritten as

$$\begin{aligned}\dot{\mathbf{Q}}(t) = \mathbf{W}_0(t)\mathbf{Q}(t) + \mathbf{W}_1(t)\mathbf{Q}(t-\tau_1) \\ +\mathbf{W}_2(t)\mathbf{Q}(t-\tau_2) + \begin{Bmatrix} 0 \\ \bar{\kappa}(t) \end{Bmatrix} f\tau_1 \end{aligned} \tag{21}$$

where $\mathbf{W}_0(t)$ is the coefficient matrix for the vector of present states

$$\mathbf{W}_0(t) = \begin{bmatrix} \mathbf{0} & \mathbf{I} \\ -\mathbf{M}^{-1}(\mathbf{K} - \hat{\kappa}(t)) & -\mathbf{M}^{-1}(\mathbf{C} - \hat{\mathbf{C}}(t)) \end{bmatrix} \tag{22}$$

and $\mathbf{W}_1(t)$ and $\mathbf{W}_2(t)$ are the coefficient matrices associated with vectors of delayed states. These matrices are given by

$$\mathbf{W}_1(t) = \begin{bmatrix} \mathbf{0} & \mathbf{0} \\ -\mathbf{M}^{-1}\hat{\kappa}_1(t)) & -\mathbf{M}^{-1}\hat{\mathbf{C}}_1(t)) \end{bmatrix} \tag{23}$$

$$\mathbf{W}_2(t) = \begin{bmatrix} \mathbf{0} & \mathbf{0} \\ -\mathbf{M}^{-1}\hat{\kappa}_2(t)) & -\mathbf{M}^{-1}\hat{\mathbf{C}}_2(t)) \end{bmatrix} \tag{24}$$

The matrices $\mathbf{W}_0(t)$, $\mathbf{W}_1(t)$, and $\mathbf{W}_2(t)$ contain T-periodic functions. Unlike the previous work reported in [9–11], multiple regenerative effects are not considered here due to the limitation of the stability analysis presented in the next section. Again, as pointed out earlier, it is mentioned that in earlier studies [2, 4, 5, 7, 8], the feed term in system (21) was not considered or dropped prior to the stability analysis.

3 Stability analysis

The system of Equation (21) is a nonlinear, nonhomogeneous, and nonautonomous delay-differential equations with time-periodic coefficients. For a chosen set of control parameters, which here are the spindle speed and the axial depth of cut (ADOC), the stability of periodic motions of this system of equations is to be determined. In this section, the semi-discretization method presented by Insperger and Stépán [14, 15] is used to determine the local stability of a periodic motion. This method is extended here to handle systems with two discrete time delays, and further, this scheme is applied to a system with loss-of-contact nonlinearities.

Let the nominal periodic solution of Equation (21) be represented by $\mathbf{Q}_0(t)$. Then, a perturbation $\mathbf{X}(t)$ is provided to this nominal solution resulting in

$$\mathbf{Q}(t) = \mathbf{Q}_0(t) + \mathbf{X}(t) \tag{25}$$

After substituting Equation (25) into Equation (21), the resulting system governing the perturbation is given by

$$\dot{\mathbf{X}}(t) = \mathbf{W}_0(t)\mathbf{X}(t) + \mathbf{W}_1(t)\mathbf{X}(t-\tau_1) + \mathbf{W}_2(t)\mathbf{X}(t-\tau_2) \tag{26}$$

The extended Floquet theory presented by Hahn [13] and Farkas [16] provides a basis for determining the stability of the trivial solution $\mathbf{X}(t) = \mathbf{0}$ of the system (26). If all of the Floquet multipliers are within the unit circle, then the corresponding periodic solution of (21) is stable. If one or more of the Floquet multipliers are on the unit circle, while the rest of them are inside the unit circle, then the corresponding periodic solution may undergo a bifurcation [17]. A difficulty with systems such as (26) is in determining the monodromy matrix [17], which has no closed-form solutions. Here, an approximation for this monodromy matrix is sought by using the semi-discretization method, and the eigenvalues of this matrix will be used to examine the local stability of the considered periodic solution.

Next, the formulation of the semi-discretization method is presented. In this formulation, the time period T of the periodic orbit is first broken up into $(k+1)$ intervals each of length Δt, and in each interval, the nonautonomous delay-differential system (26) is replaced by an autonomous ordinary differential system.

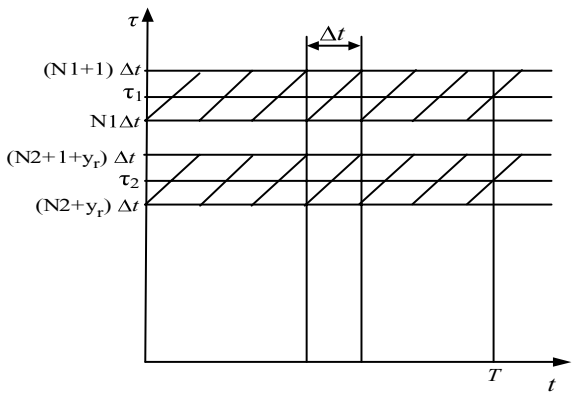

Fig. 2 Discretization scheme

This piecewise linear system of ordinary differential equations is solved to obtain a high-dimensional linear map, which is examined for determining the stability of $\mathbf{X}(t) = \mathbf{0}$ of the system (26).

As illustrated in Fig. 2, the time interval Δt is chosen as [14]

$$\Delta t = \frac{\tau_1}{N1 + (1/2)} \tag{27}$$

where $N1$ is an integer approximation. The relationship between Δt and the other discrete time delay τ_2 is given by

$$\tau_2 = \left(N2 + \frac{1}{2} + y_r\right) \times \Delta t \tag{28}$$

where y_r is given by

$$y_r = \text{mod}\left(\frac{\tau_2 - (1/2)\Delta t}{\Delta t}\right) \tag{29}$$

and

$$N2 = \frac{\tau_2}{\Delta t} - y_r - \frac{1}{2} \tag{30}$$

For $t \in [t_i, t_{i+1}]$, the delayed states are approximated as

$$\mathbf{X}(t-\tau_1) \simeq \mathbf{X}(t_i + (1/2)\Delta t - \tau_1) = \mathbf{X}(t_{i-N1}) \tag{31}$$

$$\mathbf{X}(t-\tau_2) \simeq \mathbf{X}(t_i + (1/2)\Delta t - \tau_2) = \mathbf{X}(t_{i-N2-y_r}) \tag{32}$$

$$\simeq (1-y_r)\mathbf{X}(t_{i-N2}) + y_r \cdot \mathbf{X}(t_{i-N3}) \tag{33}$$

and $N3 = N2 + 1$.

The time-periodic terms in Equation (26) are approximated as

$$\mathbf{W}_{i,0} = \mathbf{W}_0(t_i) \simeq \frac{1}{\Delta t}\int_{t_i}^{t_{i+1}} \mathbf{W}_0(t)dt \tag{34}$$

$$\mathbf{W}_{i,N1} = \mathbf{W}_{N1}(t_i) \simeq \frac{1}{\Delta t}\int_{t_i}^{t_{i+1}} \mathbf{W}_1(t)dt \tag{35}$$

$$\mathbf{W}_{i,N2} = \mathbf{W}_{N2}(t_i) \simeq \frac{1-y_r}{\Delta t}\int_{t_i}^{t_{i+1}} \mathbf{W}_2(t)dt \tag{36}$$

$$\mathbf{W}_{i,N3} = \mathbf{W}_{N3}(t_i) \simeq \frac{y_r}{\Delta t}\int_{t_i}^{t_{i+1}} \mathbf{W}_2(t)dt \tag{37}$$

Then, over each time interval $t \in [t_i, t_{i+1}]$ for $i = 0, 1, 2, \ldots, k$, Equations (26) can be approximated as

$$\begin{aligned}\dot{\mathbf{X}}(t) = {} & \mathbf{W}_{i,0}\mathbf{X}(t) + \mathbf{W}_{i,N1}\mathbf{X}_{i-N1} \\ & + \mathbf{W}_{i,N2}\mathbf{X}_{i-N2} + \mathbf{W}_{i,N3}\mathbf{X}_{i-N3}\end{aligned} \tag{38}$$

where $\mathbf{X}(t_i)$ has been rewritten as $\mathbf{X}_i$. Thus, the infinite-dimensional system (26) has been replaced by a piecewise system of ordinary differential equations in the time period $t \in [t_0, t_0 + T]$. Note that in each interval, the autonomous system has a constant excitation or forcing term that arises due to the delay effects.

To proceed further, it is assumed that $\mathbf{W}_{i,0}$ is invertible for all i. Then, the solution of Equations (38) takes the form

$$\begin{aligned}\mathbf{X}(t) = {} & e^{\mathbf{W}_{i,0}(t-t_i)}\left[\mathbf{X}_i + \mathbf{W}_{i,0}^{-1}\sum_{j=1}^{N1}\mathbf{W}_{i,j}\mathbf{X}_{i-j}\right] \\ & -\mathbf{W}_{i,0}^{-1}\sum_{j=1}^{N1}\mathbf{W}_{i,j}\mathbf{X}_{i-j}\end{aligned} \tag{39}$$

where $\mathbf{W}_{i,j} = 0$ for $j \neq N1, N2$, and $N3$. When $t = t_{i+1}$, the system (39) leads to

$$\mathbf{X}_{i+1} = \mathbf{M}_{i,0}\mathbf{X}_i + \sum_{j=1}^{N1}\mathbf{M}_{i,j}\mathbf{X}_{i-j} \tag{40}$$

where the associated matrices are given by

$$\mathbf{M}_{i,0} = e^{\mathbf{W}_{i,0}\Delta t} \tag{41}$$

and for $j > 0$,

$$\mathbf{M}_{i,j} = \begin{cases}(e^{\mathbf{W}_{i,0}\Delta t} - I)\mathbf{W}_{i,0}^{-1}\mathbf{W}_{i,j} & \text{if } j = N1, N2, N3 \\ 0 & \text{otherwise}\end{cases} \tag{42}$$

The system (40) can be used to construct the state vector

$$\mathbf{Y}_i = (\mathbf{X}_i, \mathbf{X}_{i-1}, \ldots, \mathbf{X}_{i-N1})^{\mathrm{T}} \tag{43}$$

and the linear map

$$\mathbf{Y}_{i+1} = \mathbf{B}_i\mathbf{Y}_i \tag{44}$$

where the $\mathbf{B}_i$ matrix is given by

$$\mathbf{B}_i = \begin{bmatrix}\mathbf{M}_{i,0} & \mathbf{0} & \cdots & \mathbf{M}_{i,N2} & \mathbf{M}_{i,N3} & \cdots & \mathbf{0} & \mathbf{M}_{i,N1} \\ \mathbf{I} & \mathbf{0} & \cdots & \mathbf{0} & \mathbf{0} & \cdots & \mathbf{0} & \mathbf{0} \\ \mathbf{0} & \mathbf{I} & \cdots & \mathbf{0} & \mathbf{0} & \cdots & \mathbf{0} & \mathbf{0} \\ \vdots & \vdots & \ddots & \vdots & \vdots & \ddots & \vdots & \vdots \\ \mathbf{0} & \mathbf{0} & \cdots & \mathbf{I} & \mathbf{0} & \cdots & \mathbf{0} & \mathbf{0} \\ \mathbf{0} & \mathbf{0} & \cdots & \mathbf{0} & \mathbf{I} & \cdots & \mathbf{0} & \mathbf{0} \\ \vdots & \vdots & \ddots & \vdots & \vdots & \ddots & \vdots & \vdots \\ \mathbf{0} & \mathbf{0} & \cdots & \mathbf{0} & \mathbf{0} & \cdots & \mathbf{I} & \mathbf{0}\end{bmatrix} \tag{45}$$

For a "small" feed rate, $\tau_1 \leq \tau_2 + \Delta t$, and hence, $N1 = N3$. In this case, the matrix $\mathbf{B}_i$ can be shown to be

$$\mathbf{B}_i = \begin{bmatrix}\mathbf{M}_{i,0} & \mathbf{0} & \cdots & \mathbf{M}_{i,N2} & \mathbf{M}_{i,N3} + \mathbf{M}_{i,N1} \\ \mathbf{I} & \mathbf{0} & \cdots & \mathbf{0} & \mathbf{0} \\ \mathbf{0} & \mathbf{I} & \cdots & \mathbf{0} & \mathbf{0} \\ \vdots & \vdots & \ddots & \vdots & \vdots \\ \mathbf{0} & \mathbf{0} & \cdots & \mathbf{I} & \mathbf{0}\end{bmatrix} \tag{46}$$

From the system (44), it follows that

$$\mathbf{Y}_{k+1} = \mathbf{B}_k \cdots \mathbf{B}_1\mathbf{B}_0\mathbf{Y}_0 \tag{47}$$

from which the transition matrix can be identified as

$$\mathbf{\Phi} = \mathbf{B}_k \cdots \mathbf{B}_1\mathbf{B}_0 \tag{48}$$

This matrix $\mathbf{\Phi}$ represents a finite-dimensional approximation of the "monodromy matrix" associated

Table 1 Modal parameters of workpiece–tool system

Mode	Frequency (Hz)	Damping (%)	Stiffness (N/m)	Mass (kg)
Tool (X)	1006.58	1.0	8.0×10^5	2.0×10^{-2}
Tool (Y)	1027.34	1.5	1.0×10^6	2.4×10^{-2}
Workpiece (U)	503.29	1.0	1.0×10^6	1.0×10^{-1}
Workpiece (V)	711.76	1.0	3.0×10^6	1.5×10^{-1}

Table 2 Tool and cutting parameters

Normal rake angle (ϕ_n)	Helix angle (η)	Tooth number	Radius (mm)	K_t (MPa)	k_n	Cutting friction coefficient (μ)
15°	30°	2	6.35	600	0.3	0.2

with the periodic orbit $\mathbf{Q}_0(t)$ of (21) and the trivial solution $\mathbf{X}(t) = \mathbf{0}$ of (26). If the eigenvalues of this matrix are all within the unit circle, then the trivial fixed point of (26) is stable, and hence, the associated periodic orbit of (21) is stable. At a bifurcation point, one or more of the eigenvalues of the transition matrix will be on the unit circle. Here, this information is used to determine when a period-doubling bifurcation or a secondary Hopf bifurcation is imminent.

4 Results and discussion

In this section, results obtained through numerical investigations into the dynamics and stability of various milling operations are presented. The workpiece–tool system modal parameters are shown in Table 1, and the tool and cutting parameters are shown in Table 2. The feed rate is fixed at 0.102 mm per tooth for all different cases. For comparison, the stability charts generated by using time-domain simulations [9, 11] and an averaged coefficients method is presented. The latter is labeled with the legend "averaged coefficients" in the stability charts. These stability charts are presented in the space of ADOC and the spindle speed. For the semi-discretization analysis, the periodic orbit is numerically generated from (1). In formulating the averaged coefficients method, the periodic coefficients in system (26) are averaged over one period of the orbit. The averaged coefficients method may be viewed as an approximation of the semi-discretization method where the time averaging is carried over segments spread over the period of the orbit.

The stability charts for a full immersion operation are presented in Fig. 3. The stability lobes determined

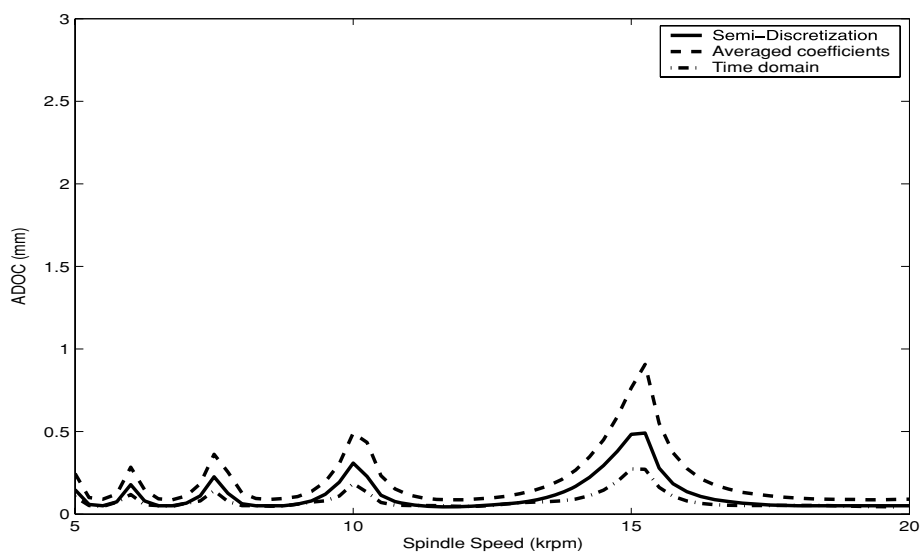

Fig. 3 Stability charts for full immersion operations

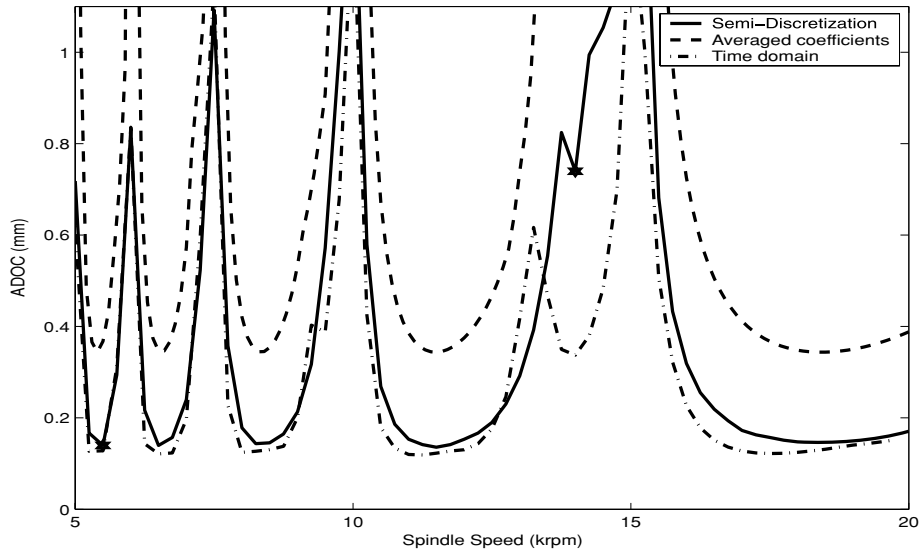

Fig. 4 Stability charts for 25% immersion up-milling operations

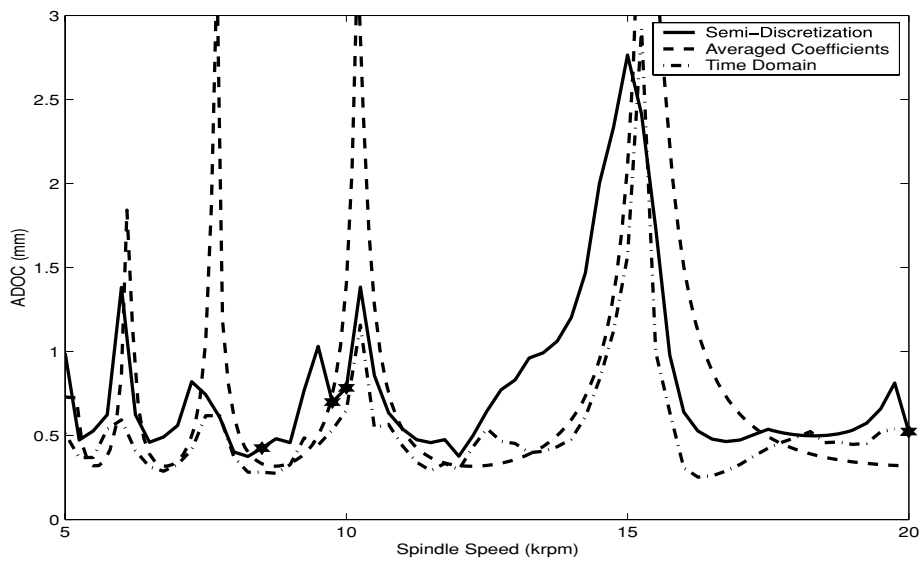

Fig. 5 Stability charts for 25% immersion down-milling operations

by time-domain simulations mark the transition from periodic motions to quasi-periodic motions of the system (1). The stability lobes determined by the averaged coefficients method are the loci of Hopf bifurcation points of the time-averaged autonomous system derived from (1). The stability lobes determined through the semi-discretization method are the loci of secondary Hopf bifurcation points. The stability chart determined by the semi-discretization method is close to the stability chart generated through time-domain simulations, while the stability chart generated by linear analysis is not close to these stability charts, especially at high spindle speeds. This may be due to a combination of two aspects, one being the averaging carried out over one complete cycle of the orbit, and the second is to do with neglect of the feed rate effect during the stability analysis. It is remarked that the feed rate term is retained in the time-domain simulations and the analysis based on the semi-discretization method.

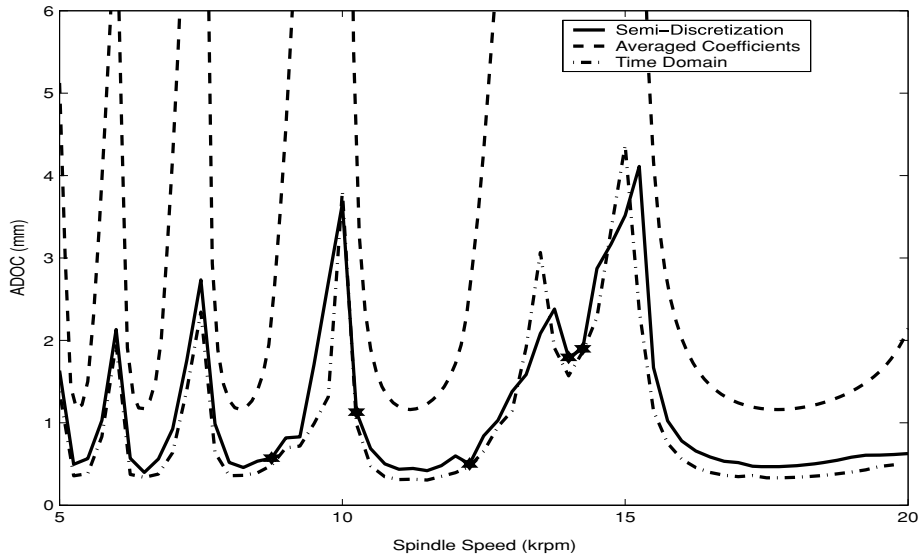

Fig. 6 Stability charts for 10% immersion up-milling operations

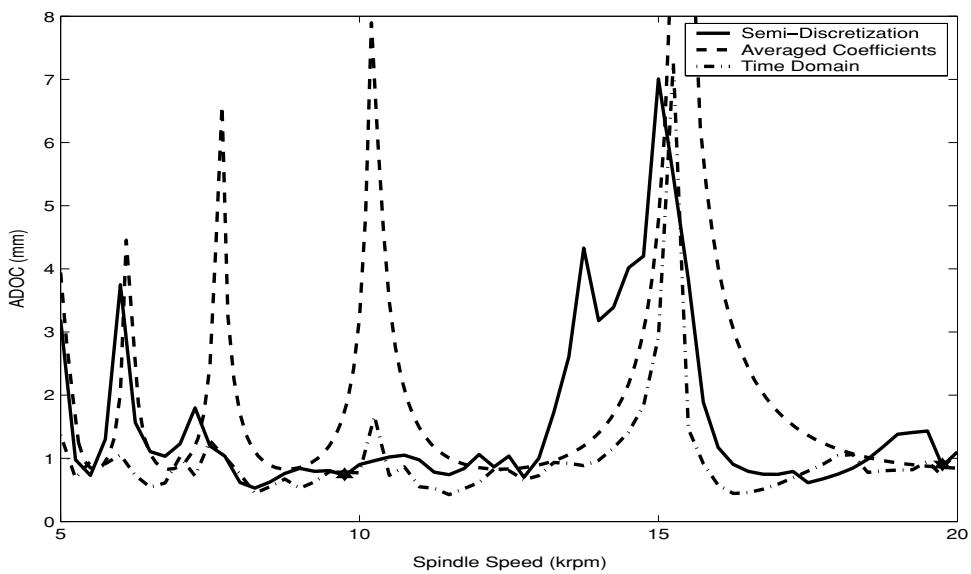

Fig. 7 Stability charts for 10% immersion down-milling operations

The stability charts for different low-immersion operations are presented in Figs. 4–7. As the immersion percentage of the tool into the workpiece decreases, the loss-of-contact effects become more prominent in the workpiece–tool system dynamics. Figures 4 and 5 correspond to up-milling and down-milling operations (i.e., opposite directions of spindle rotation) at 25 % immersion, respectively. Figures 6 and 7 represent a similar pair of results for 10% immersion, respectively. As first reported by Zhao and Balachandran [11], stability charts generated for up-milling operations and down-milling operations can be different, and this is confirmed by the results presented in Figs. 4–7. In addition, the occurrence of period-doubling bifurcation is indicated by time-domain simulations and confirmed by the results of the semi-discretization analysis. The period-doubling bifurcation points are marked by stars in the figures. At other locations on the stability lobes, secondary Hopf bifurcations occur. Due to the nature of the formulation of the averaged coefficients method,

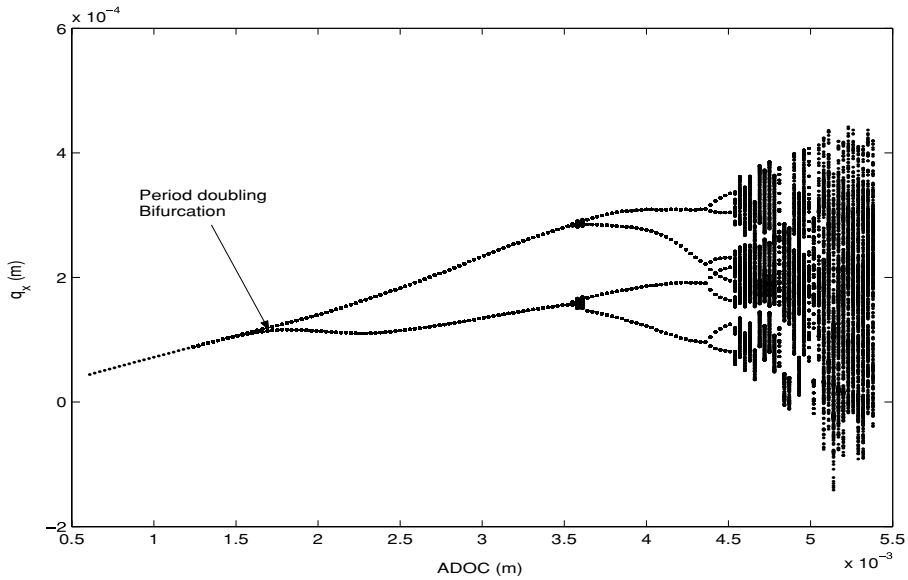

Fig. 8 Bifurcation diagram on Poincaré section for 14,200 rpm, 10% immersion up-milling operations

period-doubling bifurcations cannot be picked up by this method. In addition, as indicated in the charts for up-milling operations, the stable regions predicted by the averaged coefficients methods is much larger than that predicted by both time-domain simulations and the stability analysis based on the semi-discretization method.

In Fig. 8, for a fixed spindle speed, the numerically generated bifurcation diagram is shown when the ADOC is used as a control parameter. The first period-doubling bifurcation occurs at ADOC $= 1.87$ mm, as pointed out in Fig. 6. The Poincaré sections used for this bifurcation diagram are constructed by using the period of the orbit as the clock period.

This paper presents an attempt at using the semi-discretization method for examining the stability of milling operations. The development of this method for a system with two discrete time delays is described. Through representative examples, it is shown that this scheme predicts stability charts in fairly good agreement with those obtained by using time-domain simulations. In addition, this scheme indicates that apart from secondary Hopf bifurcations of periodic orbits, period-doubling bifurcations of periodic orbits can occur in low-immersion operations. A point to note is that the stability analysis based on the semi-discretization scheme is less time consuming compared to the time-domain simulations.

Acknowledgements Support received for this work from the National Science Foundation through Grant No. DMI-0123708 is gratefully acknowledged.

References

1. Nayfeh, A.H., Mook, D.T.: Nonlinear Oscillations. Wiley, New York (1979)
2. Tlusty, J., Polacek, M.: The stability of the machine tool against self-excited vibration in machining. In: Proceedings of the Conference on International Research in Production Engineering. Pittsburgh, PA, pp. 465–474 (1963)
3. Tobias, S.A.: Machine–Tool Vibration. Wiley, New York (1965)
4. Opitz, H., Dregger, E.U., Roese, H.: Improvement of the dynamic stability of the milling process by irregular tooth pitch. In: Proceedings of the 7th International MTDR Conference. Pergamon Press, New York (1966)
5. Sridhar, R., Hohn, R.E., Long, G.W.: A stability algorithm for the general milling process. ASME J. Eng. Ind. **90**, 330–334 (1968)
6. Hanna, N.H., Tobias, S.A.: A theory of nonlinear regenerative chatter. ASME J. Eng. Ind. **96**, 247–255 (1974)
7. Minis, I., Yanushevsky, R.: A new theoretical approach for the prediction of machine tool chatter in milling. ASME J. Eng. Ind. **115**, 1–8 (1993)
8. Altintas, Y., Budak, E.: Analytical prediction of stability lobes in milling. Ann. CIRP **44**, 357–362 (1995)
9. Balachandran, B.: Nonlinear dynamics of milling processes. Philos. Trans. R. Soc. Lond. A **359**, 793–819 (2001)
10. Balachandran, B., Zhao, M.X.: A mechanics based model for study of dynamics of milling operations. Meccanica **35**, 89–109 (2000)

11. Zhao, M.X., Balachandran, B.: Dynamics and stability of milling process. Int. J. Solids Struct. **38**(10–13), 2233–2248 (2001)
12. Balachandran, B., Gilsinn, D.: Nonlinear oscillations of milling. Math. Comput. Model. Dyn. Syst. **11**, 273–290 (2005)
13. Hahn, W.: On difference-differential equations with periodic coefficients. J. Math. Anal. Appl. **3**, 70–101 (1961)
14. Insperger, T., Stépán, G.: Semi-discretization of delayed dynamical systems. In: Proceedings of DETC'01 ASME 2001 Design Engineering Technical Conference and Computers and Information in Engineering Conference. Pittsburgh, PA, September 9–12 (2001), CD-ROM, DETC2001/VIB-21446
15. Insperger, T., Stépán, G.: Semi-discretization method for delayed systems. Int. J. Numer. Methods Eng. **55**, 503–518 (2002)
16. Farkas, M.: Periodic Motions. Springer-Verlag, Berlin Heidelberg New York (1994)
17. Nayfeh, A.H., Balachandran, B.: Applied Nonlinear Dynamics: Analytical, Computational, and Experimental Methods. Wiley, New York (1995)